RSC Advances

PAPER

View Article Online
View Journal | View Issue

Cite this: *RSC Adv.*, 2025, **15**, 49714

Development of biobased dynamic thiol–acrylate photopolymers: 3D-printed self-healing and shape memory materials

Viranchika Bijalwan,[a] Sandra Schlögl [bc] and Sravendra Rana *[a]

Dynamic covalent bonds have revolutionized polymer science by imparting advanced properties to the polymer networks, such as autonomous repair, reprocessability, adaptability, and shape recovery. The use of biobased precursors, such as plant-derived oils and natural monomers, further enhances the sustainability and environmental compatibility of these materials. By pairing dynamic covalent bonds with biobased precursors, 3D printing technologies can produce functional materials with both high performance and reduced environmental impact. In this study, we develop biobased thiol–acrylate vitrimers tailored for 3D printing applications, specifically targeting soft active devices with self-healing and shape-memory capabilities. Utilizing a digital light processing 3D printing technique, the resin formulation contains AESBO (an acrylated epoxidized soybean oil), a glycerol-derived reactive diluent, and a thiol crosslinker to attain tunable viscoelastic properties and dynamic bond exchange reactions within the printed object. The presence of hydroxyl–ester bonds in the thiol–acrylate network enables efficiently catalysed transesterification at elevated temperature in the presence of a tin-based catalyst $Sn(Oct)_2$. Notably, $Sn(Oct)_2$ functions not only as an efficient transesterification catalyst but also as a stabilizing additive that prevents premature gelation, ensuring resin shelf-stability for over two months. Experimental analysis such as dynamic mechanical analysis (DMA), reveals the significant impact of AESBO content on glass transition temperature (T_g), mechanical performance, and network adaptability. The findings from stress relaxation experiments indicate that the printed material is capable of dissipating 63% of its initial stresses within 3.6 minutes at a temperature of 200 °C, thereby facilitating self-healing and shape reformation. The materials showed promising healing, shape memory, degradability, and reprocessing capabilities, highlighting its potential for use in soft active devices and soft robotics application.

Received 15th October 2025
Accepted 8th December 2025

DOI: 10.1039/d5ra07879b

rsc.li/rsc-advances

1. Introduction

The recent developments in 3D printing, also known as additive manufacturing, have garnered great interest from material scientists and industry professionals. From prototyping and product development to creating complex designs for the healthcare and automotive sectors, 3D printing has established a significant presence in the market.[1,2] Particularly, light-based vat photopolymerization (VP) 3D printing methods such as Digital Light Processing/Projection (DLP) and Stereolithography (SLA) offer higher precision and surface finish with better speed and efficiency than extrusion-based techniques, and are compatible with a wide variety of resin materials.[3,4] These VP printing processes use liquid resins and photopolymerize them yielding statically crosslinked covalent networks or thermosets which are generally superior in their mechanical and thermal properties. However, this static network limits its reprocessability, leading to considerable waste generation.[5] To address this issue, researchers have explored dynamic bonds, such as dynamic covalent and non-covalent networks, which can be processed with a range of 3D printing processes.[6–8] Dynamic covalent networks consist of bonds that can reorganize under a suitable stimulus such as temperature, pH, or light. These networks can reshuffle and exchange their bonds, making the printed object reprocessable and adaptable similar to thermoplastics while retaining their mechanical properties like thermosets.[9–13] Dynamic networks, which rely on associative bond exchange reactions, maintain a fixed network connectivity throughout the reshuffling of bonds and therefore crosslink points remains more or less constant. At lower temperatures, this reshuffling of bonds proceeds slowly, and the materials exhibit the characteristics of thermosets. The bonds exchange at an accelerated rate above a specific temperature, referred to as the topological freezing transition temperature (T_v). This

[a]*UPES, School of Engineering, Energy Acres, Bidholi, Dehradun 248007, India. E-mail: srana@ddn.upes.ac.in; Tel: +91-9720524191*

[b]*Polymer Competence Center Leoben GmbH, Sauraugasse 1, Leoben, Austria*

[c]*Institute of Chemistry of Polymeric Materials, Technical University of Leoben, Otto Glöckel-Strasse 2, Leoben, Austria*

causes rearrangements in the network topology, allowing for viscoelastic flow which follows the Arrhenius law, a distinctive characteristic of dynamic polymer networks.[14–16] Such dynamic polymers possess advanced features such as repairability, reprocessability, and self-adaptability, enabling the material to be recycled, which in turn extends the polymer material's usability and lifetime.

Several dynamic covalent exchange chemistries have been explored, such as transesterification,[17,18] carbamate bond exchange,[19] imine exchange,[20,21] disulfide exchange,[22,23] boronate–ester bond exchange,[24,25] pyrazole–urea bond exchange,[26,27] Diels–Alder exchange,[28,29] and many more. In 3D printing, however, the most popular exchange chemistry is the transesterification mechanism of hydroxyl–ester groups, which is highly versatile and related materials are processable by various printing techniques such as DLP, SLA, and Fused Filament Fabrication (FFF).[30–32] Thiol–acrylate networks are emerging as a promising class of materials for designing DLP-printable vitrimers that rely on transesterification chemistry (Fig. 1). The hydroxyl & ester linkages in the network (within the acrylate and thiol moieties) not only impart mechanical strength but also enable dynamic transesterification reactions, thereby promoting relaxation of internal stresses and self-healing in the printed material.[33–35] Thiol–acrylate networks are superior to thiol–ene networks as photopolymers due to their faster polymerization, which is attributed to the combination of thiol–acrylate copolymerization and acrylate homopolymerization. The thiol groups serve as chain transfer agents for homopolymerization, and their addition reduces inhomogeneities in the network, resulting in a more uniform crosslink density and improved properties of the material.[36,37]

While transesterification may proceed without the need of a catalyst (*e.g.* by introducing activated ester moieties), the majority of the reported dynamic networks require a catalyst. 1,5,7-triazabicyclo(4.4.0)dec-5-ene (TBD), triphenylphosphine (TPP), and zinc(II) acetylacetonate ($Zn(acac)_2$) are a few examples of transesterification catalysts where the latter is the most extensively applied in 3D printing.[38–40] Gao *et al.*[31] developed recyclable vitrimers using SLA 3D printing by combining exchangeable β-hydroxyl esters and sacrificial hydrogen bonds in an acrylate prepolymer, and they utilized TBD to catalyse the thermoactivated transesterification. $Zn(acac)_2$ has also been used as an efficient transesterification catalyst in light-mediated 3D printing for faster stress relaxation of networks allowing for the production of repairable and reprocessable objects.[17,41] The limited solubility of aforementioned catalysts in some acrylate-based systems poses challenges for photopolymerization-based 3D printing. To address this, Schlögl *et al.* introduced liquid organic phosphates and phosphonates in their work, which dissolve readily in most acrylate resins and serve as efficient transesterification catalysts.[38,42] These facilitated rapid stress relaxation at elevated temperatures, crucial for the printed objects to exhibit dynamic features. A tin-based catalyst tin(II) 2-ethylhexanoate ($Sn(Oct)_2$) has previously been used to catalyse thermoactivated transesterification reactions in thiol–epoxy networks by Hayashi *et al.*[43] Since $Sn(Oct)_2$ is a liquid catalyst, it

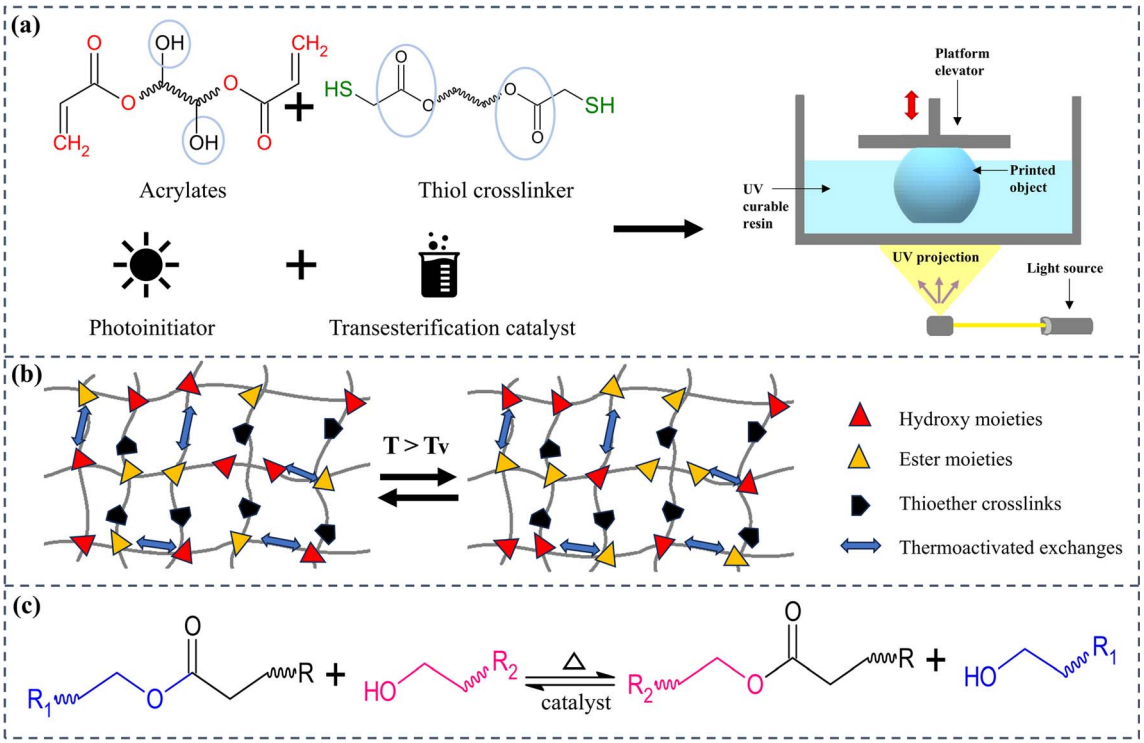

Fig. 1 (a) Generalised structure and schematics of the thiol–acrylate based resin composition used for the digital light processing (DLP) 3D printing. The highlighted hydroxyl and ester groups indicate the functional groups that participate in the dynamic transesterification, (b) schematic representation of a crosslinked thiol–acrylate network undergoing dynamic transesterification above its T_v, (c) exchange mechanism of hydroxyl and ester groups at elevated temperatures during transesterification in the presence of a catalyst.

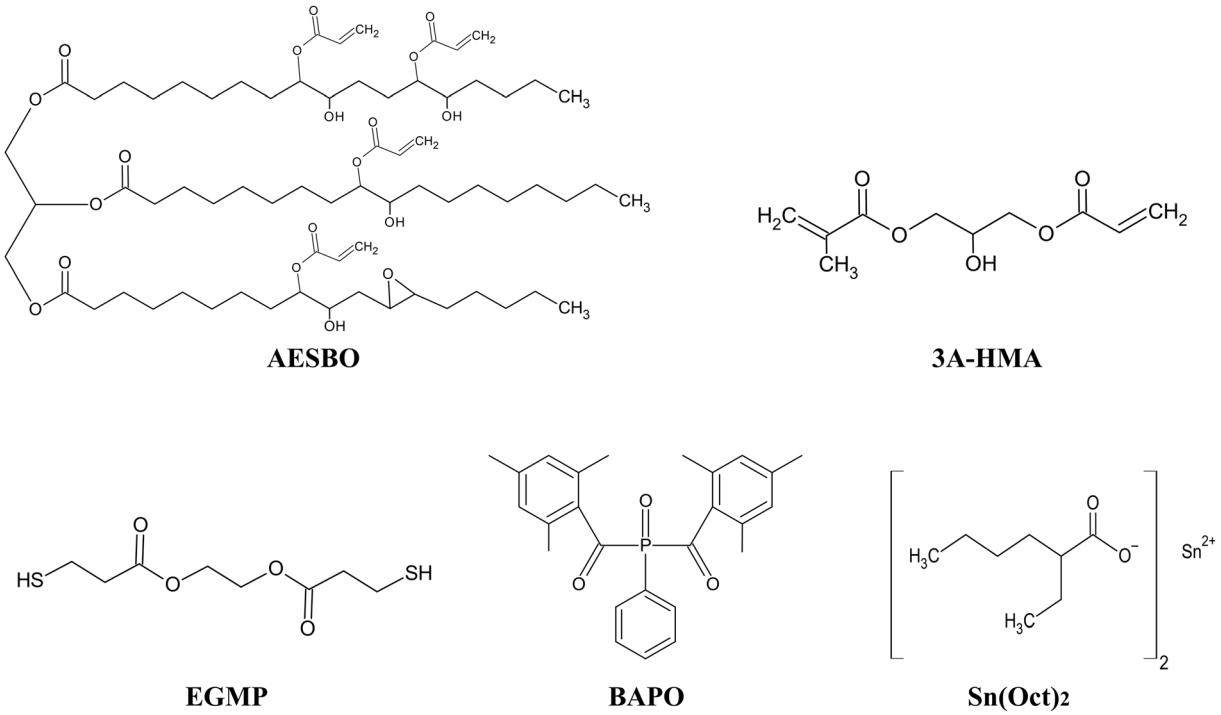

Fig. 2 Chemical structures of components of the resin formulation: acrylated epoxidized soybean oil (AESBO), 3-(acryloyloxy)-2-hydroxypropyl methacrylate (3A-HMA), ethylene glycol bis(3-mercaptopropionate) (EGMP), phenylbis(2,4,6-trimethylbenzoyl)phosphine oxide (BAPO), and tin(II) 2-ethylhexanoate ($Sn(Oct)_2$).

can be also easily solubilized in acrylate resins and give a homogenized mixture of monomers even when added at room temperature and therefore is compatible with DLP 3D printing resins.[44]

Concurrently, biobased dynamic polymer networks have been a new focus for researchers in recent years to reduce the dependence on fossil resources and further minimize the carbon footprint. Since petrochemicals are a source for most of the traditional dynamic networks, biobased ones from renewable sources such as plant oils, lignin, vanillin, glycerol, and furan derivatives have gained attention.[45–47] Vegetable oils derived from seeds such as castor, soybean, and linseed oil are also promising choices for starting materials in vat photopolymerization 3D printing since they possess unsaturation in their glyceride groups, which can be modified and polymerized.[48–50] These unsaturated moieties can be oxidized into epoxides, and further, these epoxides can easily be converted to acrylate groups on successful reaction with acrylic acid. Such vegetable oil-based acrylates are suitable for free-radical polymerization under (UV) light triggered by the photoinitiator present in the printing resin. Glycerol is another biobased compound that is a derivative of biodiesel synthesis and originates from renewable resources such as vegetable oils or animal fats. In many studies, glycerol-based monomers possessing hydroxyl and ester groups necessary for transesterification have also been employed in the 3D printing of dynamic polymer networks.[51–53]

In this work, we developed biobased UV-curable thiol–acrylate resins which serve as a versatile platform for creating transesterification-based dynamic polymer networks processable with DLP 3D printing. We incorporated $Sn(Oct)_2$ as a liquid transesterification catalyst. Taking photopolymerization 3D-printing one step closer to the sustainability targets desired by mankind, we propose to use acrylated soybean oil (AESBO) synthesized from a fully bio-based epoxidized oil (ESBO). Furthermore, 3-(acryloyloxy)-2-hydroxypropyl methacrylate (3A-HMA), which is derived from glycerol, was used as reactive viscosity modifier/diluent to lower the viscosity of AESBO during printing. The effect on the curing kinetics, viscosity, and rheological properties of the printing resins is studied by varying concentrations of AESBO and 3A-HMA. By carefully designing the composition of the resin formulation and taking advantage of the thiol–ene click reaction, photopolymers with reversible dynamic bonds were obtained. The chemical structures of the components comprising the DLP printing resin are depicted in Fig. 2. The resulting 3D printed structures exhibited rapid thermoactivated network rearrangements as demonstrated by stress relaxation experiments. The printed materials demonstrated self-repair, shape reforming properties, reprocessability, recycling properties. The goal is to achieve customizable, functional materials with enhanced durability, sustainability, and adaptability for applications in soft robotics/actuators, and wearable technology.

2. Experimental

2.1. Materials

Butylated hydroxytoluene (BHT) was purchased from Thermo Fischer. Ethylene glycol bis(3-mercaptopropionate) (EGMP) and the photoinitiator phenylbis(2,4,6-trimethylbenzoyl)phosphine

oxide (BAPO) were supplied by TCI Chemicals. Acrylic acid, tin(II) 2-ethylhexanoate ($Sn(Oct)_2$), 3-(acryloyloxy)-2-hydroxypropyl methacrylate (3A-HMA), and triphenylphosphine (TPP) were procured from Sigma-Aldrich. Epoxidized soybean oil (ESBO) was obtained by KLJ Group, Haryana Enterprises, India.

2.2. Synthesis of acrylated soybean oil

AESBO was prepared from 0.40 mol of ESBO (30.0 g) by reacting it with 0.80 mol of acrylic acid (4.58 g) in a round-bottomed flask fitted with a thermometer, reflux condenser, and nitrogen inlet. To prevent unwanted radical polymerization during the reaction, 0.09% by weight of BHT (0.027 g) was added to suppress free radical formation. Then, 1% by weight of TPP (0.3 g) as a catalyst was added.[54] This reaction was continued overnight while the temperature was increased to 80–85 °C. Following reaction completion, the product was brought to room temperature, diluted with diethyl ether, and subsequently purified by repeatedly washing it with deionized water until a neutral pH was attained. The product was dried to remove any remaining water and solvent completely (synthesis steps are provided in Fig. S1 – SI).

2.3. Preparation of resin formulations

At 50 °C, the photoinitiator BAPO (2.5 wt%) was added and stirred in various weight ratios of AESBO until it was dissolved in the mixture. After cooling the resin to room temperature, various amounts of a reactive diluent (3A-HMA) were incorporated, along with 5 wt% $Sn(Oct)_2$ as a transesterification catalyst. Lastly, the thiol crosslinker EGMP (20 wt%) was added to the formulation and stirred till a homogeneous mixture was achieved. The synthesized resins were stored in amber glass vials to prevent light exposure. Table 1 provides an overview of the various DLP printing formulations, their compositions, and properties, and Table 2 gives the acrylate to thiol ratio of all the biobased resin formulations.

2.4. DLP 3D printing

DLP printing of the 3D was carried out using an Anycubic Photon D2 printer (Shenzhen, China) equipped with a UV LED 405 nm light source. The initial 8 layers were cured for 90 seconds, while the subsequent layers were illuminated for 80 seconds, determined by the optimal monomer conversion analyzed through FTIR spectroscopy. The printing process was conducted with a layer resolution of 50 μm, a 2 mm s^{-1} building speed, and a 2 mm s^{-1} retracting speed. An Anycubic Wash and Cure Station was used to rinse all the printed samples with ethanol and post-cure them for 5 minutes.

2.5. Material characterization

A PerkinElmer Frontier FT-IR spectrometer was used to examine the real-time conversion of ESBO to AESBO using Fourier transform infrared spectroscopy. Reaction progress over illumination time was monitored for all the resin samples. At a resolution of 4 cm^{-1}, 16 scans were collected in transmission mode during each exposure period between 4000 and 400 cm^{-1}. Photocuring reactions were analyzed by exposing the resin to light radiation within the 250–450 nm wavelength range. Acrylate (absorbance peak at 1635 cm^{-1}) and the thiol group (absorbance peak at 2570 cm^{-1}) conversions were estimated from characteristic peak areas at the corresponding exposure dose. FT-IR spectra of original sample, chemically recycled (120 °C in ethylene glycol, 20 h), and mechanically reprocessed samples (120 °C, 50 min at 1 bar) were recorded using a PerkinElmer, Spectrum Two spectrometer with a diamond ATR (attenuated total reflection) module. Each sample was analyzed with 16 scans over a spectral range of 4000–400 cm^{-1}.

The viscosity of the resins was measured using a modular compact rheometer (Anton Paar MCR 92, Austria) fitted with a bob and cup accessory. Each measurement of the resin sample was performed on 10 mL of resin at room temperature (25 °C) across a 0.1 to 300 s^{-1} shear rate range.

A TMA instrument (TA-Q400EM) was used in three-point bending mode on printed rectangular specimens (15 × 7 × 2 mm) to perform stress relaxation and stress–strain experiments. A 0.01 N preloaded force was used to straighten the sample during the stress relaxation test, which was conducted at temperatures between 140 to 200 °C. After applying the required temperature along with 1% strain during testing, the relaxation modulus was determined in relation to time. Three replicates were recorded for every data point in the Arrhenius graph. At a constant temperature of 40 °C and a 0.02 N force, stress–strain tests were conducted in strain ramp mode.

To determine the storage modulus and tan δ of the rectangular printed specimens (15 × 5 × 2 mm), three-point bending tests were performed on a DMA 850 (TA Instruments). Using 3 °C min^{-1} heating rates and a 50 mL min^{-1} nitrogen purge gas flow, the storage modulus and tan δ were determined over a −40 °C to 120 °C temperature range. A 0.2 N force was used in

Table 1 Composition of the investigated DLP resin formulations along with their viscosity (at 25 °C), gel content, and T_g

Resin	AESBO (wt%)	3A-HMA (wt%)	EGMP (wt%)	BAPO (wt%)	$Sn(Oct)_2$ (wt%)	Viscosity (mPa s)	Gel content (%)	T_g (DMA) (°C)
ASG10	10	60	20	2.5	5	192 ± 6	96	53
ASG20	20	50	20	2.5	5	227 ± 10	92	38
ASG30	30	40	20	2.5	5	271 ± 3	86	31
ASG40	40	30	20	2.5	5	371 ± 5	80	20
ASG50	50	20	20	2.5	5	691 ± 6	76	0
ASG60	60	10	20	2.5	5	1149 ± 15	70	0

Table 2 The acrylate to thiol mol. ratio for the resin formulations

Resin formulation	Total acrylate (AESBO + diluent) (mol%)	Total thiol (mol%)	Mol. ratio of acrylate : thiol
ASG10	0.580	0.168	3.45 : 1
ASG20	0.506	0.168	3.01 : 1
ASG30	0.420	0.168	2.50 : 1
ASG40	0.350	0.168	2.08 : 1
ASG50	0.288	0.168	1.71 : 1
ASG60	0.210	0.168	1.25 : 1

these experiments, and the glass transition temperatures (T_g) were identified from the peak of the tan δ curve.

Thermogravimetric analysis (TGA) was conducted utilizing a PerkinElmer TGA 4000 equipment to assess the thermal stability of the polymers. The samples were heated in a nitrogen atmosphere, at a constant rate of 10 °C min^{-1} from 30 to 700 °C.

The gel content was assessed by immersing 0.2 g of DLP 3D-printed polymer samples in dichloromethane (DCM). Dry samples (W_0) were subjected to a 48-hour extraction in 5–10 mL of DCM. Subsequently, the samples were removed and dried in an oven at 40 °C until they achieved a constant weight and then reweighed (W_1). The gel content was estimated by using the following equation:

$$\text{Gel content (\%)} = (W_1/W_0) \times 100 \quad (1)$$

2.6. Self-healing experiments

For the healing experiment, rectangular specimens (15 × 7 × 2 mm) including a control sample, a sample with a circular defect (4 mm), and a matching 4 × 2 mm circular disc were 3D printed using the ASG50 resin. The circular discs were inserted within the cavity of the defective sample and heated at 180 °C for 5 hours to evaluate their self-healing ability. Stress–strain measurements were then performed on the control, defective (with hole), and thermally healed samples using a TMA instrument (TA-Q400EM). The self-healing behavior of the printed and light-cured ASG50 sample was also investigated by scratching it with a razor blade. Subsequently, it was heated in an oven at 150 °C for 1 hour, and 180 °C for 2 hours, and the crack was examined using an optical microscope (Olympus BX51). The healing efficiency was estimated based on the initial scratch width (W_i) and final scratch width (W_f) by using the formula:

$$\text{Healing efficiency (\%)} = ((W_i - W_f)/W_i) \times 100 \quad (2)$$

2.7. Shape-reforming experiments

Shape reforming experiments were conducted using a 3D-printed ASG50 rectangular specimen and a sample printed as a "gripper" structure. The shape-memory response was evaluated by heating these samples above their T_v, bending them into a temporary shape, and cooling them above their T_g. For programming a second transient shape, the samples were further reshaped and rapidly quenched in a cold bath (below T_g) to maintain the deformation. When heated again over its T_v, the sample recovered its original permanent form, demonstrating triple shape-memory.

2.8. Chemical recycling experiments

The chemical degradation and recycling properties were tested by immersing the ASG50 sample in 10 mL of ethylene glycol at 120 °C. Samples were collected at regular intervals (hourly), then dried and weighed. The difference in mass before and after degradation of the sample was used to determine the relative weight. The degraded product was assessed using Fourier Transform Infrared (FTIR) spectroscopy.

2.9. Reprocessability experiments

The 3D-printed ASG50 specimens were cut into smaller pieces. The resulting material was molded into a sheet with a hot press and heated at 120 °C for 50 min, applying 1 bar pressure. After reaching room temperature, the recycled material was cut into rectangular specimens for mechanical testing. The recycled material was again fragmented and reprocessed under same conditions for another cycle of recycling. The stress–strain behavior of specimens after both reprocessing cycles were then evaluated by TA-Q400EM and compared with the virgin ASG50 sample.

3. Results

3.1. Evaluation of photocuring kinetics and network properties of dynamic thiol–acrylate photopolymers

Epoxidized soybean oil (ESBO) was used in the synthesis of AESBO as received. The supplier reported an oxirane oxygen content of 6.5 ± 0.1 wt% (ASTM-D-1652). Based on this value, the corresponding epoxy equivalent weight was determined to be ≈246 g per eq. using the standard oxirane-oxygen method for epoxidized oils.[55] This value was used directly for all molar calculations required for synthesizing AESBO from ESBO. The acrylation was carried out through a catalyst-mediated ring-opening reaction with acrylic acid to yield acrylated soybean oil AESBO. The synthesis of AESBO was verified by ^{1}H NMR spectroscopy using deuterated chloroform ($CDCl_3$) as solvent (Fig. S2 and S3). The methylene group (CH_2) protons situated between two carbon–carbon double bonds in the fatty acid chains of AESBO appear at 2.0–2.5 ppm (H_h). The chemical shifts observed at 5.76, 6.29–6.34, and 6.02–6.06 ppm correspond to the protons of the acrylate group (CH_2=CH–),

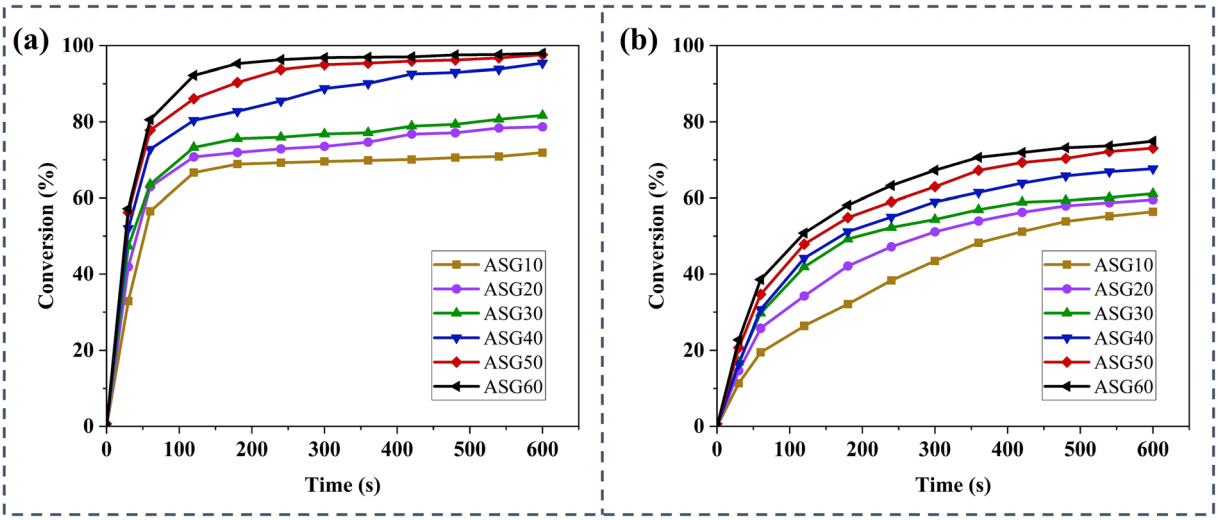

Fig. 3 (a) Acrylate conversion and (b) thiol conversion percentage of different resin compositions at 1635 cm^{-1} and 2570 cm^{-1} respectively, over illumination time (600 s) as obtained from FTIR experiments (irradiation was carried out under air). The lines are a guide for the eye.

specifically the protons of the vinyl moiety (H_c, H_a) and the methylene proton (H_b) in the CH_2–CH– moiety.[56] Notably, the characteristic epoxy group signal around 3 ppm is also diminished in the NMR spectrum of AESBO. The absorption bands of the glycerol backbone (H_d, H_e) due to its four methylene protons at 4.0–4.3 ppm remain unchanged during acrylation and were therefore used as an internal standard reference to determine both epoxy conversion and number of acrylate functionality in AESBO.[57,58] By normalizing their integral to a value of 4 (corresponding to 4 protons), an epoxy conversion of 92.7% was estimated leaving a residual epoxide functionality of 0.54. This indicated that a small fraction of epoxides did not form acrylate esters, likely due to minor side reactions or partial hydrolysis.[48] The same internal reference integral was used to estimate the acrylate functionality by comparing the vinyl proton integrals (H_a, H_b, H_c), yielding an acrylate functionality of 2.54 for AESBO.[58] This functionality was adequate for the subsequent thiol–acrylate curing reactions, and further increasing the epoxy conversion was therefore not required.

All FTIR spectra were baseline-corrected and normalized prior to analysis. Functional group conversion was quantified based on peak height integration of the characteristic absorption bands. The FTIR spectrum shown in Fig. S4 indicates the absence of the peak of the epoxy doublet at 842 and 822 cm^{-1} from AESBO, which was originally present in the epoxidized oil (ESBO). The appearance of the vinyl peak (986 cm^{-1}) and the characteristic vibrational band corresponding to stretching at 1635 cm^{-1}, of the acrylic carbon double bond, further confirms the presence of acrylate groups in the synthesized AESBO. The presence of the acrylic carbon double bond is also indicated by an additional absorption peak at 810 cm^{-1}, corresponding to the bending vibration of the C=C bond in the acrylic vinyl segment.[56]

The bifunctional thiol, EGMP, was used to prepare AESBO–thiol resins and create thiol–acrylate networks by light-induced thiol–ene reaction. Given its broad absorption spectrum, BAPO, used as a Norrish type I photoinitiator, allowed the AESBO-resins to cure when exposed to UV-visible light. Viscosity is a crucial property for resins in vat-photopolymerization 3D printing since it affects the material's flow, layer formation, and overall printability. The viscosity of resins used for 3D printing generally ranges between 200 and 1500 mPa s.[49] The incorporation of the reactive diluent (3A-HMA) into the AESBO resins was aimed at lowering the overall viscosity to enhance the resin's flow properties, making it more appropriate for DLP 3D printing. Resin formulations were prepared with varying mass ratios between 3A-HMA and AESBO whilst keeping the thiol content constant at 20 wt%. As the amount of reactive diluent increases and the amount of AESBO decreases, the resins' viscosity decreases (Table 1). The viscosity ranged from 192 to 1150 mPa s in resin samples across ASG10 to ASG60 (Fig. S5). These resins exhibit good storage stability as no gelation was observed in the printing resins after being stored for 2 months in the dark (Fig. S6). This behavior could be attributed to the presence of $Sn(Oct)_2$, which acts effectively as both a transesterification catalyst and a stabilizing agent, thus preventing premature gelation of thiol–acrylate resins typically observed within a few days. The curing behavior of the formulated resins was examined by monitoring the reduction of the distinctive stretching bands at 2570 cm^{-1} (associated with thiol S–H bonds) and 1635 cm^{-1} (C=C deformation linked to the acrylate group) over the duration of light exposure. Fig. S7 in the SI shows FTIR spectra of the resin before and after 10 minutes of light irradiation. The final acrylate conversion was much higher in all six resin formulations, ranging from 72% to 98%, whereas the thiol conversion varied between 56% and 74% in compositions across ASG10 to ASG60 (Fig. 3(a and b)). This disparity is due to the acrylate groups being involved in two simultaneous reaction pathways: the acrylate chain-growth homopolymerization and the thiol–acrylate step-growth copolymerization, resulting in a hybrid reaction mechanism.[33,37,52]

Upon exposure to UV-visible light, the Norrish type I photoinitiator undergoes homolytic cleavage, producing reactive radicals. Radical initiation abstracts a thiol group hydrogen, forming a thiyl radical that attacks the acrylate double bond to create a radical that is carbon-centered.[59,60] This radical can either abstract another thiol hydrogen, following a step-growth mechanism, or add to an acrylate moiety, initiating a chain-growth mechanism. The chain-growth progresses rapidly, leading to the formation of high molecular weight molecules, whereas step-growth polymerization tends to generate lower molecular weight compounds. This causes delayed gelation and reduced shrinkage stress, resulting in the formation of a more homogeneous polymer network.[36] In ASG60 and ASG50, the acrylate moieties achieved a maximum conversion of 98%, while ASG10 showed a lower conversion of around 72% after 10 minutes of illumination. This difference in conversion rates can be attributed to several factors. The reactive diluent having a lower molecular weight introduces more functional groups per unit mass, but the higher methacrylate content in ASG10 results in lower intrinsic reactivity compared to acrylate groups. Additionally, diffusion limitations that arise during polymerization may also inhibit conversion in a more densely functional system. Therefore, ASG10 has a lower overall conversion even though it has higher functionalization. The optimized viscosity and reactivity of the biobased thiol–acrylate resin allowed smooth recoating and its defect-free printing. The efficient light absorption at 405 nm of the resin allowed rapid curing and yielded parts with good dimensional accuracy. Good adhesion between printed layers and negligible shrinkage were observed, indicating high compatibility of the biobased formulation with the DLP printing process. 3D structures of various shapes could be printed using the biobased resin formulations (Fig. 4(a–c) and S8). Printed parts were rinsed with ethanol to remove any uncured residue and then post-cured for 5 min using an Anycubic Wash and Cure Station.

To determine the extent of crosslinking within the printed thiol–acrylate network, the gel content of 3D-printed samples was measured. After being immersed in dichloromethane for 48 hours, the cured samples were weighed dry to estimate the insoluble fraction. The gel content of the samples ranged from 96% to 70% across ASG10–ASG60 (Table 1), indicating that the relative composition of AESBO and the glycerol-based diluent significantly influenced the network structure. An increase in AESBO content resulted in a lower gel content, whereas, incorporating glycerol as a reactive diluent enhanced crosslink density, leading to a more tightly crosslinked polymer network. This decrease in gel content can be attributed to the reduced crosslinking efficiency of AESBO compared to the glycerol-based reactive diluent due to its bulky/branched triglyceride structure resulting in a lower effective concentration of reactive groups and stearic effects during network formation. In addition, its flexible, plasticizing alkyl chains results in larger chain mobility during curing, further decreasing the probability of efficient crosslinked network formation. Whereas, the reactive diluent provides higher available functional group as they are less sterically hindered. Therefore, formulations with higher reactive diluent content exhibit a higher insoluble network fraction or gel content.

3.2. Mechanical and thermal properties of the dynamic thiol–acrylate photopolymers

The thermomechanical properties of printed thiol–acrylate photopolymers were then examined. DMA curves revealed a progressive rise in the storage modulus (G') across samples ASG60 to ASG10, *i.e.*, with the decrease of AESBO content in the printed structures (or the increasing amount of the glycerol-based reactive diluent) (Fig. 5(a)). The rigidity of the printed polymer samples was therefore improved by increasing the reactive diluent content in the resins. This was an outcome of the formation of a highly interconnected network upon the addition of the reactive diluent, as was also reported in similar studies.[49,51] ASG10 and ASG20 maintain the highest G' across the temperature range, indicating greater stiffness and elastic behavior of the printed material. The storage modulus of samples printed with resins ASG30 to ASG60 is significantly lower, particularly ASG50 and ASG60 transition to rubbery state at lower temperatures suggesting lower glass transition temperature (T_g) values. Furthermore, they are softer and more compliant. The initial slight increase in G' from −40 to −20 °C for samples may be attributed to the lower molecular mobility

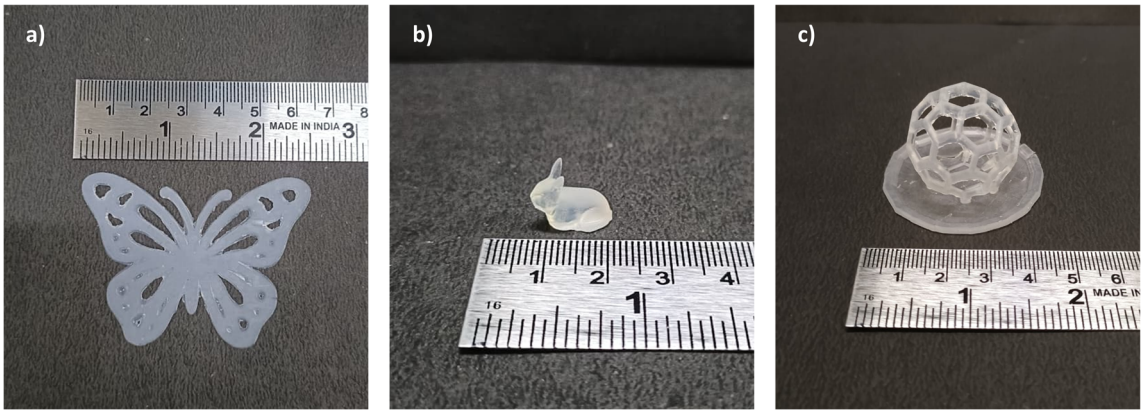

Fig. 4 3D structures of a (a) butterfly, (b) rabbit, and (c) fullerene, printed using the thiol–acrylate resin.

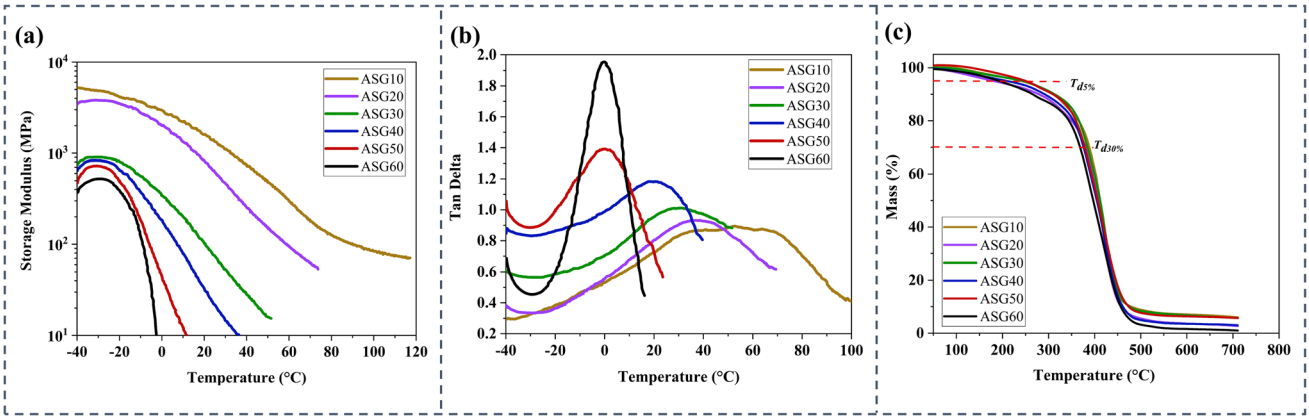

Fig. 5 Plots depicting (a) the storage modulus (G') as a function of temperature and (b) the tan δ variation with temperature, and (c) thermogravimetric (TGA) curves for different 3D printed dynamic thiol–acrylate photopolymers.

of the polymer chains at very low temperatures, where the network behaves in a more glassy and rigid state. As the temperature approaches −20 °C, these constrained segments slightly stiffen under the applied oscillatory deformation, resulting in a rise in G' in those samples. The further decrease in G' is due to the onset of the glass transition region of the flexible AESBO-based segments. Within this temperature range, the increase in thermal energy enables segmental relaxation, causing the material to transition from a rigid glassy state to a softer viscoelastic state. This was also confirmed by correlating the T_g of the printed materials obtained with their tan δ curves (Fig. 5(b)). The T_g values for the printed dynamic polymer networks show a decrease across samples ASG10 to ASG60, where ASG10 has a T_g of 53 °C whereas ASG50 and ASG60 exhibit T_g values approaching 0 °C. As AESBO content increases, the crosslink density of the network decreases because AESBO has flexible aliphatic chains that introduce more free volume and chain mobility into the network. Higher AESBO incorporation also results in an increase in the molecular weight between two crosslink points, which further reduces network rigidity and the observed reduction in T_g for ASG50 and ASG60. Because of this flexibility, the material is less rigid, which lowers the T_g of the ASG50 and ASG60 samples. These properties make them ideal for applications where flexibility and adaptability to external forces are desired, such as soft robotics. Lower T_g values can also be associated with the flexibility-enhancing effect of AESBO monomers in the network, particularly at higher weight percentages. The flexible aliphatic chains in AESBO disrupt the densely packed polymer network, thus enhancing chain mobility and resulting in a lower T_g. The thermostability of the thiol–acrylate printed photopolymers was investigated using TGA, and the outcomes are depicted in Fig. 5(c). The temperature at a weight loss of 30% ($T_{d,30\%}$) for all the printed thiol–acrylate samples ranges from 368 to 388 °C, where the ASG10 sample shows the highest temperature for $T_{d,30\%}$. Despite the relatively lower conversion observed for ASG10, its high $T_{d,30\%}$ indicates minimal presence of unreacted acrylate monomers within the network, suggesting that the formed structure remains thermally rigid and well crosslinked. Overall, all samples exhibit high thermal stability and resistance to degradation at higher temperatures.

3.3. Stress-relaxation behavior of the dynamic thiol–acrylate photopolymers

The static covalent bonds of thermosets make their stress relaxation difficult even at increased thermal conditions, whereas the exchange reactions of the dynamic covalent adaptable networks at high temperatures enable rapid stress release from any deformation.[61] Therefore, to study these topology rearrangements, the topology freezing transition (T_v) temperature was determined by analyzing the stress relaxation response of the samples. The topological rearrangement within printed thiol–acrylate photopolymers, driven by dynamic hydroxyl–ester bonds facilitating transesterification, was studied using stress relaxation tests in TMA. Fig. 6(a) depicts the stress relaxation response of various 3D printed samples at 140 °C. The relaxation time (τ) represents the duration needed for the stress or modulus to reduce to $1/e$ (37%) of its original value.[62] The relaxation times for the 3D-printed samples decrease across samples ASG60 to ASG10 at 140 °C, with all except ASG60 reach stress relaxation under 60 minutes at this temperature. Noticeably, the stiffer ASG10 network exhibited the fastest relaxation, which can be attributed to its higher 3A-HMA content, introducing more hydroxyl and ester groups that actively participate in transesterification. This trend indicates that the stress relaxation rate is primarily governed by the concentration of dynamic bonds rather than by chain mobility, as formulations with lower 3A-HMA content (ASG50 and ASG60) showed slower relaxation despite their increased flexibility. Additionally, the high catalytic efficiency of $Sn(Oct)_2$ effectively accelerates the transesterification reactions, further contributing to the observed faster relaxation kinetics. Because of its high acrylate and thiol conversions, ideal viscosity, lower storage modulus values suitable for soft devices, and ability to achieve stress relaxation within reasonable time, the sample printed with resin ASG50 was chosen to demonstrate applications for soft active devices.

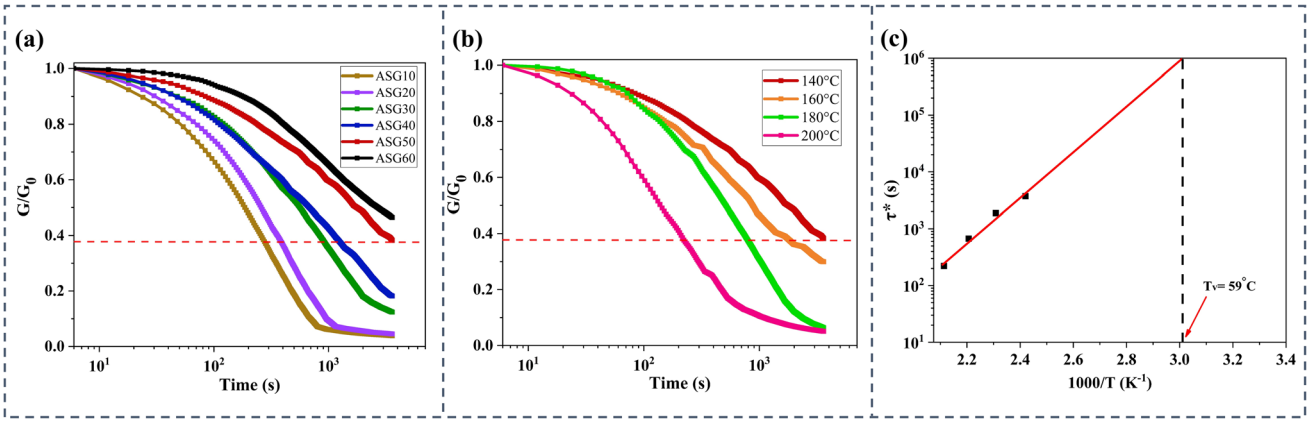

Fig. 6 (a) Stress relaxation curves (normalized) for different 3D-printed dynamic thiol–acrylate photopolymers recorded at 140 °C, (b) stress relaxation curves (normalized) for 3D-printed ASG50 obtained at a temperature range from 140 °C to 200 °C, (c) Arrhenius curve for 3D-printed ASG50 demonstrating a linear relationship, characteristic of an associative bond exchange in the dynamic polymer network.

Since the exchange reactions of dynamic bonds are temperature-dependent, heating the sample further accelerates these reactions. Temperature-dependent stress relaxation curves of the ASG50 sample are shown in Fig. 6(b). The τ value of ASG50 reduces from 58 minutes at 140 °C to just 3.6 minutes as the temperature increases to 200 °C. This decrease in relaxation times results from the accelerated exchange rate of transesterification at higher temperatures and the enhanced mobility of molecular chain segments, which facilitates faster rearrangement.[16] As depicted in Fig. 6(c), a linear trend is observed for τ values of ASG50 which align well with the Arrhenius expression $\tau^* = \tau_0 \exp(E_a/RT)$, and confirms the dynamic behavior of the thiol–acrylate network (where E_a = activation energy, R = gas constant, and T = temperature).[62,63] The data can be extrapolated to a relaxation time of 10^6 in the Arrhenius plot to estimate the value of T_v.[52,62] Using this, the T_v for the ASG50 sample was calculated to be 59 °C from the Arrhenius plot, which was found to be similar to other such soybean oil and glycerol-based dynamic polymers (66 °C).[49] Using the slope of the linear fit ($m = E_a/R$), the networks' activation energy (E_a) was found to be 76.7 kJ mol^{-1} (Fig. S9 in SI).

3.4. Self-healing properties

The fast exchange of dynamic bonds above their T_v gives soft active materials additional functions such as inherent healing ability. For this, the thermo-responsive healing and repair capabilities of 3D-printed ASG50 samples were evaluated. A rectangular specimen with a central circular defect (hole) and one without a hole (control sample) were DLP 3D-printed. A

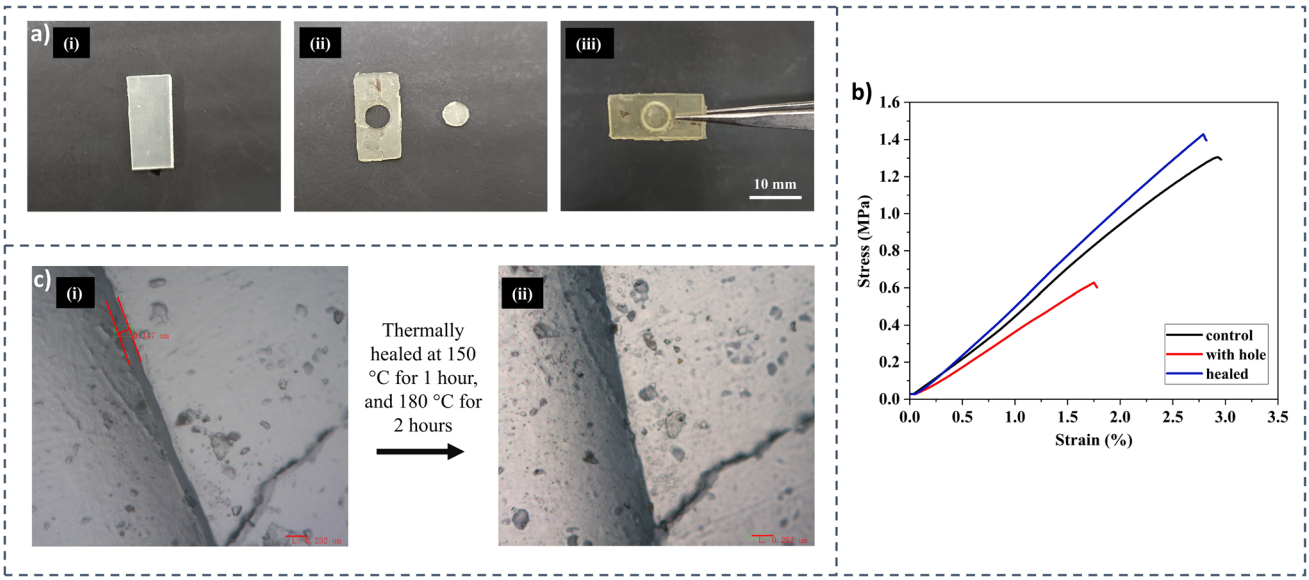

Fig. 7 (a) (i) Control specimen, (ii) defective specimen (featuring a 4 mm circular defect and a 4 mm disc), and (iii) thermally healed specimen of the 3D-printed ASG50. (b) Stress–strain graph of the control, defective (with hole), and healed specimens. (c) Optical images of a scratched surface (width: 0.147 μm) of the 3D-printed ASG50 sample (i) prior and (ii) after thermally treating at 150 °C for 1 hour, and 180 °C for 2 hours.

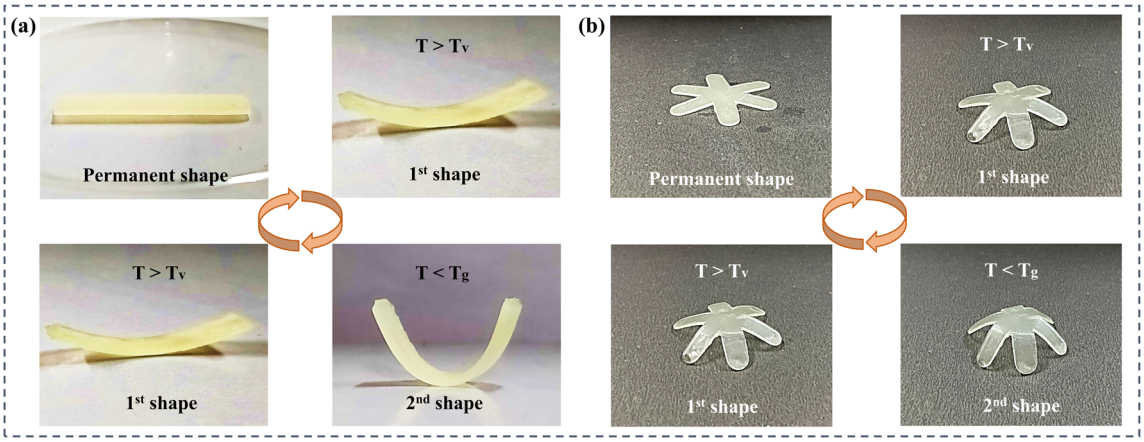

Fig. 8 Digital photographs representing the triple shape memory behavior of DLP 3D-printed ASG50 samples: (a) rectangular sample and (b) flower-shaped "gripper" sample, when programmed above their T_v.

matching disc was printed and inserted into the cavity of the defective sample (Fig. 7(a)). The heat-induced healing for this sample was carried out at 180 °C for 5 hours since stress relaxation studies revealed a lower τ above this temperature.

Flexural tests of the healed ASG50 specimen produced stress–strain curves closely matching those of the control sample, highlighting the superior healing efficiency of the ASG50 thiol–acrylate network (Fig. 7(b)). The healed sample showed a steeper slope in the curve than the control sample, thus indicating a slightly higher elastic modulus and stiffness, achieving a 1.42 MPa peak stress observed at a strain of around 2.7%. Additionally, a scratch repair test was also performed for ASG50 samples to validate the self-healing of the printed object. A scratch was made on the surface of the printed specimen using a razor blade and subsequently thermally treated at 150 °C for 1 hour, and 180 °C for 2 hours. A healing efficiency of 76% was calculated from the width of the repaired and scratched sample after 1 hour of thermal treatment. Whereas, after another 2 hours, only the scar of the original scratch is visible on the surface, indicating nearly full recovery (Fig. 7(c)). These experiments demonstrated the ASG50 network to repair efficiently due to the dynamic ester exchange process and structural network reconfiguration above T_v upon contact.

3.5. Shape reforming properties

The 3D-printed ASG50 sample has flexible AESBO chains and free hydroxyl groups that provide plasticity and support the shape memory or reforming function. 3D structures of various shapes could be printed using the ASG50 resin. The dynamic thiol–acrylate networks also allow the printed sample to exhibit triple shape memory when heated and programmed above its transition temperatures (T_g and T_v).[64] Shape reforming experiments were conducted using a 3D-printed ASG50 rectangular specimen and a sample printed as a "gripper" structure. The process involves four sequential steps. Step 1: the ASG50 printed structures were first heated above their T_v (80 °C), and manually shaped and deformed. Step 2: the deformed structure was then cooled to 30 °C (which is above T_g), to fix the first transient shape. Step 3: then, for the second transient shape, the specimen was further deformed and then the sample was quickly quenched in a cold bath (below T_g), to restrict segmental motion. Step 4: to regain the permanent shape, the sample was simply heated above T_g, and the permanent shape was fully recovered (Fig. 8(a and b)). Thus, the material demonstrates good shape memory, as hydroxyl groups enabled plasticity, locking the molecular chains during cooling and restoring flexibility when reheated. The material demonstrated a recovery time of just 1 min to regain its permanent shape, highlighting the potential of these 3D-printed dynamic thiol–acrylate photopolymers for thermally actuated soft active devices application.

3.6. Chemical recycling

Recycling polymeric products is essential to address environmental, economic, and resource sustainability challenges. When 3D-printed polymeric materials lose their functional qualities, they must be degraded or recycled after use. Unlike thermosets, dynamic polymer networks can be recycled using chemical and mechanical methods to minimize the accumulation of plastic debris in the environment.[65] Transesterification-based dynamic polymers can be chemically regenerated using processes such as glycolysis or alcoholysis at higher temperatures.[66] Chemical degradation of the 3D-printed ASG50 sample was carried out by soaking the object in ethylene glycol at 120 °C. The weight loss curve of ASG50 as a function of temperature is shown in Fig. 9(b). After chemical recycling, the sample was shrunk into a brown mass and the colour of ethylene glycol also changed from clear to brown (Fig. 9(a)). This indicates that transesterification between ester linkages in the ASG50 and the reactive hydroxyl moieties of ethylene glycol facilitate the breakdown of the cross-linked network and thus caused the fragments to dissolve in ethylene glycol. During the first 6 hours, the sample was rapidly reduced to 50% of its initial weight, then gradually to 24% after 17 hours, and then stabilized. Some of the residue was left after chemical degradation due to the permanent linkages of the sample.[41] The intensity of

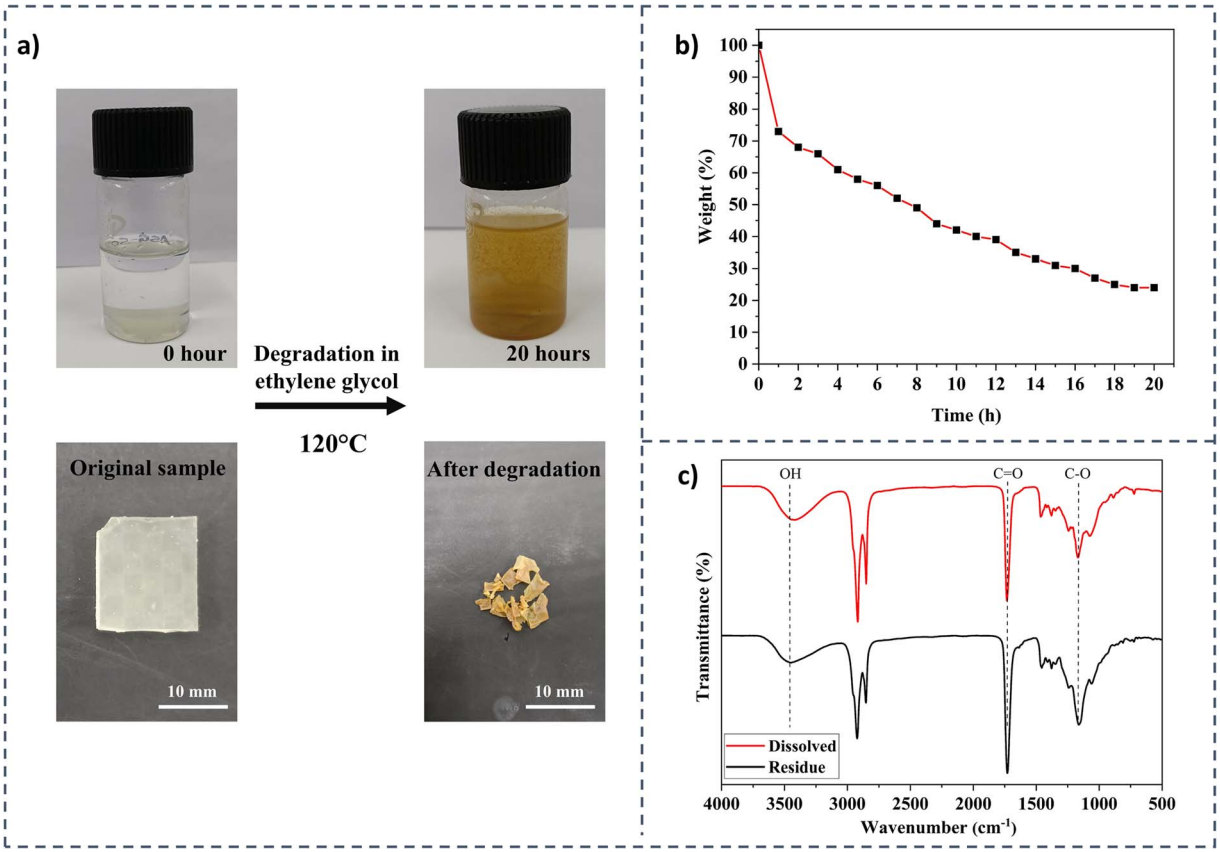

Fig. 9 (a) Chemical degradation of 3D-printed ASG50 sample in ethylene glycol over a period of 20 hours when done at 120 °C. (b) The weight loss of the 3D-printed ASG50 sample *versus* time (20 hours). (c) FTIR analysis of the sample residue following chemical recycling and its dissolution in ethylene glycol.

the O–H group FTIR signal at 3455 cm^{-1}, along with the C=O and C–O group signals from the ester moiety at 1730 and 1163 cm^{-1} remained unchanged in the ASG50 sample residue after chemical recycling and dissolution in ethylene glycol, suggesting that the remaining network structure was reorganized *via* dynamic transesterification (Fig. 9(c)).

3.7. Reprocessability properties

The 3D-printed sample was tested for reprocessability using a hot press molding machine. The printed ASG50 samples were fragmented into smaller pieces and remolded through hot pressing at 120 °C for 50 min at 1 bar pressure. A continuous sheet was rebuilt from the sample pieces, which retained its flexible nature upon bending, however, the surface of the sheet blackened due to the direct contact with the heated metal press (Fig. 10(a)). The pristine original sample exhibited a steady increase in stress with strain, indicative of its inherent flexibility and lower stiffness. After the first reprocessing cycle, the stress–strain curve of the remolded specimen showed ~1.5 times increase in the flexural strength, compared to the original ASG50 specimen, at a maximum strain of 1.5%, indicating reduced ductility after reprocessing (Fig. 10(b)). After the second reprocessing cycle, the specimen exhibited approximately twice the flexural strength compared to the original, but with further reduction in deformability, indicating enhanced stiffness but increased brittleness upon repeated thermal processing.

The improvement in mechanical performance of the reprocessed samples was attributed to the thermal treatment under applied pressure, which caused structural reorganization and additional formation of hydrogen bonds.[39] Additionally, the applied temperature and pressure densified the matrix by potential removal of internal voids. A simultaneous increase in elastic modulus and reduction in strain at break after successive reprocessing cycles confirm the formation of a more compact and rigid polymer network, and demonstrate that although the network becomes mechanically stronger, it also becomes more brittle. Thus, reprocessing results in an evolution of mechanical properties, although flexibility diminishes as stiffness increases with multiple reprocessing cycles, indicating only partial recovery of original mechanical profile.

Furthermore, a comparison between the FTIR spectra of the original and reprocessed samples revealed similar absorption peaks for the –OH group at approximately 3455 cm^{-1} and the C=O group at 1730 cm^{-1}, indicating that the chemical structure remained unchanged after reprocessing (Fig. 10(c)). Thus, the ASG50 sample demonstrated its capability to be reprocessed from its printed waste material using hot press molding techniques.

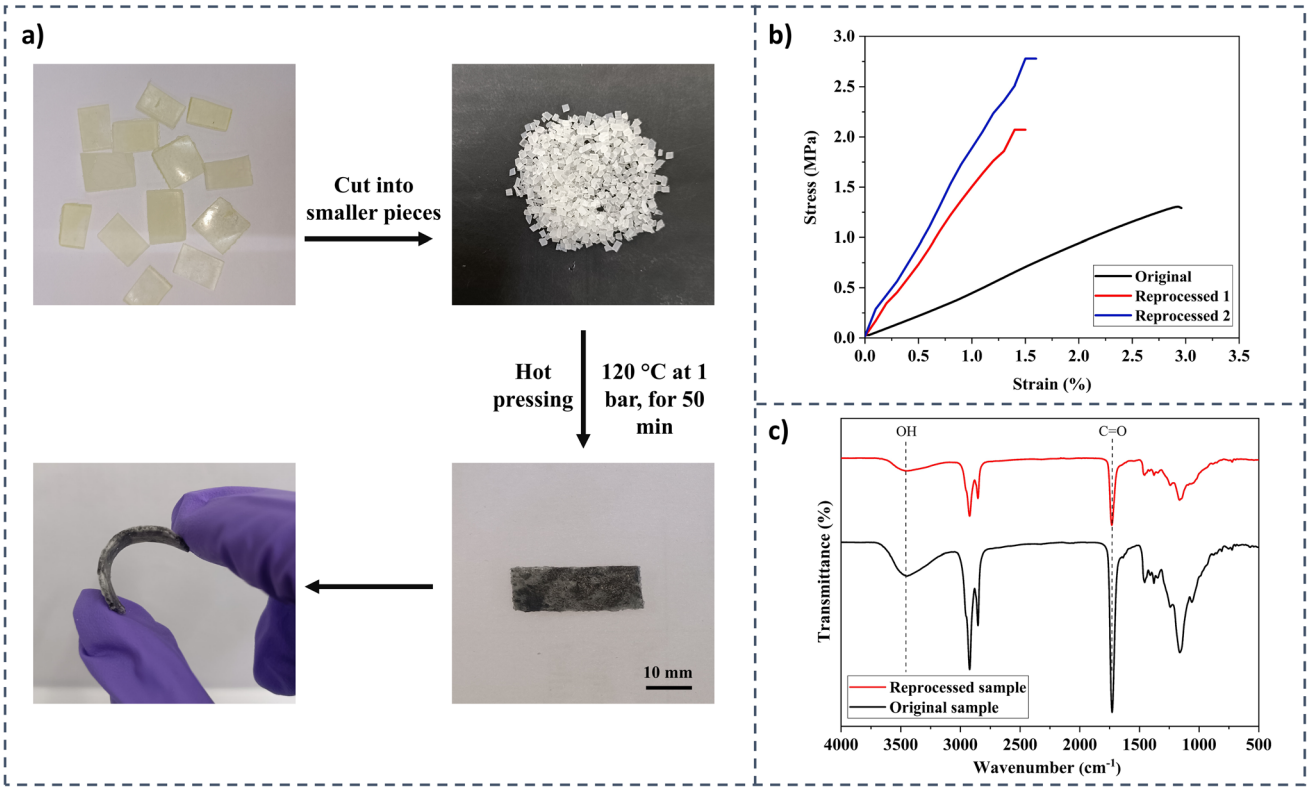

Fig. 10 (a) Reprocessing scheme of 3D-printed ASG50 sample when remolded in a hot press at 120 °C. (b) Stress–strain graph of the reprocessed ASG50 sample. (c) FTIR spectra of the original and reprocessed ASG50 sample.

4. Conclusion

Using biobased precursors derived from soybean oil and glycerol monomers, we have developed dynamic thiol–acrylate photopolymers as resins for 3D printing. Resins with varying amounts of AESBO monomer and 3A-HMA reactive diluent were prepared which printed objects having a T_g range between ~0 to 53 °C. $Sn(Oct)_2$, a liquid tin-based catalyst, was added to the thiol–acrylate resin to promote transesterification reactions and stabilize against premature gelation during storage. This dual functionality was essential for maintaining long-term resin stability and ensuring good processability of formulations. Photopolymerization studies revealed that formulations with higher AESBO content exhibited faster cure kinetics, due to higher reactivity of acrylate groups and lower diffusion constraints. Conversely, stress relaxation experiments showed that samples with lower AESBO content relaxed more rapidly, due to a higher concentration of hydroxyl and ester groups facilitating dynamic bond exchange. For further experiments, the photopolymer ASG50 was chosen having the maximum acrylate and thiol conversions (98% and 73%), suitable viscosity (691 ± 6 mPa s, attained across a shear rate range of 0.1 to 300 s^{-1}), low storage modulus and T_g values (~0 °C) ideal for soft devices, combined with the ability to achieve stress relaxation within a reasonable time. The ASG50 network exhibited faster stress relaxation with rising temperature from 140 °C to 200 °C, and the τ value decreased from 58 minutes to just 3.6 minutes. The ASG50 network exhibited healing, recyclability, and shape memory characteristics as a result of dynamic transesterification between the hydroxyl groups and ester groups of the thiol–acrylate photopolymers, activated at higher temperatures. Defective 3D printed samples could be repaired by thermally treating them at 180 °C for 5 hours and recovering their properties. The successful repair of surface scratches was also demonstrated. The printed dynamic photopolymer underwent chemical recycling through degradation in ethylene glycol at higher temperatures and was also reprocessable when remolded in a hot press, although mechanical property evolution during repeated reprocessing indicates only partial retention of the original mechanical properties, thus, limits the number of reprocessability cycles. The shape-reforming ability of the printed network also suggests its potential for applications in soft robotics and actuators, where transitions between two shapes are needed.

Author contributions

V. B.: conceptualization; organic synthesis; data curation; validation; methodology; investigation; formal analysis; writing – original draft; writing – review and editing; S. S.: validation; writing – review and editing; S. R.: conceptualization; funding acquisition; investigation; methodology; supervision; validation; writing – original draft; writing – review and editing.

Conflicts of interest

There are no conflicts to declare.

Data availability

The data supporting this article have been included as part of the supplementary information (SI), and the file for the same has been uploaded with the submission. Supplementary information is available. See DOI: https://doi.org/10.1039/d5ra07879b.

Acknowledgements

The authors would like to express their sincere gratitude to India Austria Science and Technology Cooperation (DST/IC/Austria/2024/122) for financial support. Viranchika Bijalwan would like to acknowledge the Council of Scientific & Industrial Research (CSIR), India, for providing financial support through the Senior Research Fellowship (SRF) Direct Scheme. Part of the research was carried out within the COMET-Module project "Repairtecture" (project no.: 904927) at the Polymer Competence Center Leoben GmbH (PCCL, Austria) within the framework of the COMET-program of the Federal Ministry for Climate Action, Environment, Energy, Mobility, Innovation and Technology and the Federal Ministry of Economy, Energy and Tourism. Funding was provided by the Austrian Government and the State Governments of Styria and Upper Austria.

References

1 S. C. Ligon, R. Liska, J. Stampfl, M. Gurr and R. Mülhaupt, *Chem. Rev.*, 2017, **117**, 10212–10290.
2 T. D. Ngo, A. Kashani, G. Imbalzano, K. T. Q. Nguyen and D. Hui, *Composites, Part B*, 2018, **143**, 172–196.
3 M. Pagac, J. Hajnys, Q.-P. Ma, L. Jancar, J. Jansa, P. Stefek and J. Mesicek, *Polymers*, 2021, **13**, 598.
4 A. Al Rashid, W. Ahmed, M. Y. Khalid and M. Koç, *Addit. Manuf.*, 2021, **47**, 102279.
5 V. S. D. Voet, J. Guit and K. Loos, *Macromol. Rapid Commun.*, 2021, **42**, 2000475.
6 V. S. D. Voet, *ACS Mater. Au*, 2023, **3**, 18–23.
7 V. Bijalwan, S. Rana, G. J. Yun, K. P. Singh, M. Jamil and S. Schlögl, *Polym. Rev.*, 2024, **64**, 36–79.
8 V. Bijalwan, S. Rana, S. Schlögl, W. H. Binder and G. J. Yun, *Polym. Rev.*, 2025, **65**, 975–1009.
9 P. Chakma and D. Konkolewicz, *Angew. Chem., Int. Ed.*, 2019, **58**, 9682–9695.
10 C. J. Kloxin and C. N. Bowman, *Chem. Soc. Rev.*, 2013, **42**, 7161–7173.
11 L. Porath, B. Soman, B. B. Jing and C. M. Evans, *ACS Macro Lett.*, 2022, **11**, 475–483.
12 N. Kaushik, P. Singh, S. Rana, N. G. Sahoo, F. Ahmad and M. Jamil, *Mater. Today Sustain.*, 2024, **27**, 100828.
13 H. Sharma, V. Bijalwan, A. H. I. Mourad, A. Kumar, S. Schlögl and S. Rana, *J. Reinf. Plast. Compos.*, 2024, DOI: 10.1177/07316844241295848.
14 B. Krishnakumar, R. V. S. P. Sanka, W. H. Binder, V. Parthasarthy, S. Rana and N. Karak, *Chem. Eng. J.*, 2020, **385**, 123820.
15 W. Denissen, J. M. Winne and F. E. Du Prez, *Chem. Sci.*, 2016, **7**, 30–38.
16 M. Guerre, C. Taplan, J. M. Winne and F. E. Du Prez, *Chem. Sci.*, 2020, **11**, 4855–4870.
17 B. Zhang, K. Kowsari, A. Serjouei, M. L. Dunn and Q. Ge, *Nat. Commun.*, 2018, **9**, 1831.
18 J. Casado, O. Konuray, A. Roig, X. Fernández-Francos and X. Ramis, *Eur. Polym. J.*, 2022, **173**, 111256.
19 S. Sun, X. Gan, Z. Wang, D. Fu, W. Pu and H. Xia, *Addit. Manuf.*, 2020, **33**, 101176.
20 J.-T. Miao, M. Ge, S. Peng, J. Zhong, Y. Li, Z. Weng, L. Wu and L. Zheng, *ACS Appl. Mater. Interfaces*, 2019, **11**, 40642–40651.
21 S. Kim, M. A. Rahman, M. Arifuzzaman, D. B. Gilmer, B. Li, J. K. Wilt, E. Lara-Curzio and T. Saito, *Sci. Adv.*, 2022, **8**, 6006.
22 C. Choi, Y. Okayama, P. T. Morris, L. L. Robinson, M. Gerst, J. C. Speros, C. J. Hawker, J. Read de Alaniz and C. M. Bates, *Adv. Funct. Mater.*, 2022, **32**, 2200883.
23 K. Yu, A. Xin, H. Du, Y. Li and Q. Wang, *NPG Asia Mater.*, 2019, **11**, 7.
24 L. L. Robinson, J. L. Self, A. D. Fusi, M. W. Bates, J. Read de Alaniz, C. J. Hawker, C. M. Bates and C. S. Sample, *ACS Macro Lett.*, 2021, **10**, 857–863.
25 A. J. R. Amaral, V. M. Gaspar, P. Lavrador and J. F. Mano, *Biofabrication*, 2021, **13**, 035045.
26 S. Sun, G. Fei, X. Wang, M. Xie, Q. Guo, D. Fu, Z. Wang, H. Wang, G. Luo and H. Xia, *Chem. Eng. J.*, 2021, **412**, 128675.
27 J. Wang, S. Sun, X. Li, G. Fei, Z. Wang and H. Xia, *3D Print. Addit. Manuf.*, 2023, **10**, 684–696.
28 A. Durand-Silva, K. P. Cortés-Guzmán, R. M. Johnson, S. D. Perera, S. D. Diwakara and R. A. Smaldone, *ACS Macro Lett.*, 2021, **10**, 486–491.
29 H. Ouyang, X. Li, X. Lu and H. Xia, *ACS Appl. Polym. Mater.*, 2022, **4**, 4035–4046.
30 M. Fei, T. Liu, B. Zhao, A. Otero, Y.-C. Chang and J. Zhang, *ACS Appl. Polym. Mater.*, 2021, **3**, 2470–2479.
31 H. Gao, Y. Sun, M. Wang, Z. Wang, G. Han, L. Jin, P. Lin, Y. Xia and K. Zhang, *ACS Appl. Mater. Interfaces*, 2021, **13**, 1581–1591.
32 G. Prasanna Kar, X. Lin and E. M. Terentjev, *ACS Appl. Polym. Mater.*, 2022, **4**, 4364–4372.
33 U. Shaukat, E. Rossegger and S. Schlögl, *Polymer*, 2021, **231**, 124110.
34 E. Rossegger, K. Moazzen, M. Fleisch and S. Schlögl, *Polym. Chem.*, 2021, **12**, 3077–3083.
35 U. Shaukat, A. Thalhamer, E. Rossegger and S. Schlögl, *Addit. Manuf.*, 2024, **79**, 103930.
36 C. E. Hoyle and C. N. Bowman, *Angew. Chem., Int. Ed.*, 2010, **49**, 1540–1573.
37 C. E. Hoyle, T. Y. Lee and T. Roper, *J. Polym. Sci., Part A: Polym. Chem.*, 2004, **42**, 5301–5338.
38 E. Rossegger, R. Höller, D. Reisinger, M. Fleisch, J. Strasser, V. Wieser, T. Griesser and S. Schlögl, *Polymer*, 2021, **221**, 123631.

39 S. Grauzeliene, B. Kazlauskaite, E. Skliutas, M. Malinauskas and J. Ostrauskaite, *eXPRESS Polym. Lett.*, 2023, **17**, 54–68.
40 Z. Chen, M. Yang, M. Ji, X. Kuang, H. J. Qi and T. Wang, *Mater. Des.*, 2021, **197**, 109189.
41 S. Grauzeliene, M. Kastanauskas, V. Talacka and J. Ostrauskaite, *ACS Appl. Polym. Mater.*, 2022, **4**, 6103–6110.
42 K. Moazzen, E. Rossegger, W. Alabiso, U. Shaukat and S. Schlögl, *Macromol. Chem. Phys.*, 2021, **222**, 2100072.
43 M. Hayashi and A. Katayama, *ACS Appl. Polym. Mater.*, 2020, **2**, 2452–2457.
44 V. Bijalwan and S. Rana, *Monatsh. Chem.*, 2025, DOI: 10.1007/s00706-025-03381-x.
45 J. Stouten, G. H. M. Schnelting, J. Hul, N. Sijstermans, K. Janssen, T. Darikwa, C. Ye, K. Loos, V. S. D. Voet and K. V. Bernaerts, *ACS Appl. Mater. Interfaces*, 2023, **15**, 27110–27119.
46 B. Krishnakumar, A. Pucci, P. P. Wadgaonkar, I. Kumar, W. H. Binder and S. Rana, *Chem. Eng. J.*, 2022, **433**, 133261.
47 P. Singh, W. H. Binder, P. Kumar, R. Patel, G. J. Yun and S. Rana, *ACS Appl. Mater. Interfaces*, 2024, **16**, 54693–54705.
48 U. Shaukat, B. Sölle, E. Rossegger, S. Rana and S. Schlögl, *Polymers*, 2022, **14**, 5377.
49 S. Grauzeliene, A.-S. Schuller, C. Delaite and J. Ostrauskaite, *Eur. Polym. J.*, 2023, **198**, 112424.
50 G. Zhu, J. Zhang, J. Huang, Y. Qiu, M. Liu, J. Yu, C. Liu, Q. Shang, Y. Hu, L. Hu and Y. Zhou, *Chem. Eng. J.*, 2023, **452**, 139401.
51 S. Grauzeliene, A.-S. Schuller, C. Delaite and J. Ostrauskaite, *ACS Appl. Polym. Mater.*, 2023, **5**, 6958–6965.
52 E. Rossegger, R. Höller, D. Reisinger, J. Strasser, M. Fleisch, T. Griesser and S. Schlögl, *Polym. Chem.*, 2021, **12**, 639–644.
53 H. Li, B. Zhang, R. Wang, X. Yang, X. He, H. Ye, J. Cheng, C. Yuan, Y. Zhang and Q. Ge, *Adv. Funct. Mater.*, 2022, **32**, 2111030.
54 D. Behera and A. K. Banthia, *J. Appl. Polym. Sci.*, 2008, **109**, 2583–2590.
55 J. D. Espinoza-Perez, B. A. Nerenz, D. M. Haagenson, Z. Chen, C. A. Ulven and D. P. Wiesenborn, *Polym. Compos.*, 2011, **32**, 1806–1816.
56 X. Li, D. Wang, L. Zhao, X. Hou, L. Liu, B. Feng, M. Li, P. Zheng, X. Zhao and S. Wei, *Prog. Org. Coat.*, 2021, **151**, 105942.
57 W. Xia, S. M. Budge and M. D. Lumsden, *J. Agric. Food Chem.*, 2015, **63**, 5780–5786.
58 O. Gómez-de-Miranda-Jiménez-de-Aberasturi, J. Calvo, I. Svensson, N. Blanco, L. Lorenzo and R. Rodriguez, *Molecules*, 2024, **29**, 4582.
59 M. J. Kade, D. J. Burke and C. J. Hawker, *J. Polym. Sci., Part A: Polym. Chem.*, 2010, **48**, 743–750.
60 C. E. Hoyle, A. B. Lowe and C. N. Bowman, *Chem. Soc. Rev.*, 2010, **39**, 1355.
61 M. Chen, L. Zhou, Y. Wu, X. Zhao and Y. Zhang, *ACS Macro Lett.*, 2019, **8**, 255–260.
62 M. Capelot, M. M. Unterlass, F. Tournilhac and L. Leibler, *ACS Macro Lett.*, 2012, **1**, 789–792.
63 D. Montarnal, M. Capelot, F. Tournilhac and L. Leibler, *Science*, 2011, **334**, 965–968.
64 G. Zhang, Q. Zhao, L. Yang, W. Zou, X. Xi and T. Xie, *ACS Macro Lett.*, 2016, **5**, 805–808.
65 J. Zheng, Z. M. Png, S. H. Ng, G. X. Tham, E. Ye, S. S. Goh, X. J. Loh and Z. Li, *Mater. Today*, 2021, **51**, 586–625.
66 T. Liu, B. Zhao and J. Zhang, *Polymer*, 2020, **194**, 122392.